ELSEVIER

Fluid Dynamics Research 24 (1999) 275–292

FLUID DYNAMICS RESEARCH

Fluid flow in a rotating low-specific-speed centrifugal impeller passage

F.C. Visser *, J.J.H. Brouwers [1], J.B. Jonker

Faculty of Mechanical Engineering, University of Twente, Enschede, The Netherlands

Received 17 December 1997; revised 25 June 1998; accepted 4 July 1998

Abstract

Results from experimental investigations of the blade passage flow in a model pump impeller of low specific speed are described. It is found that the flow inside the rotating impeller passages is well described by the flow distribution postulated by potential-flow arguments and boundary-layer considerations. Using a custom-designed two-component laser-Doppler-velocimetry flow measurement system, mounted on a frame co-rotating with an impeller, the radial and circumferential velocity components of the relative flow inside an impeller passage were measured. Measurements were taken from blade to blade, and from this the passagewise fluid velocity was determined. The measured passagewise fluid velocity is compared to the potential-flow solution of the impeller passage-flow velocity that holds asymptotically in a region well away from the blade tips. Additional potential-flow finite-element calculations are used for comparison for those regions where the asymptotic expansion does not hold. The agreement between the experimental and theoretical values is seen to be good for the core flow region, which extends from the blade pressure side to the viscous boundary layer at the blade suction side. Furthermore, the calculation of the boundary-layer development along the suction side of the impeller blades is highlighted. Contrary to the blade pressure side, only there a significant departure from inviscid flow behaviour is observed. Calculations performed in the ordinary fashion, i.e. employment of the common thin-shear-layer approximation, substantiate the conception that for a low-specific-speed impeller the effects of spanwise rotation and modest surface curvature are accommodated in the description of the inviscid core flow.

1. Introduction

For the purpose of better understanding and predicting the hydraulic performance of centrifugal pumps, a solid knowledge of the flow field within the impellers of this type of rotating-flow machine is needed. The current study aims to contribute to this knowledge. It focuses on the flow field that was measured inside the passages of a shrouded low-specific-speed model centrifugal impeller of

* Present address. Flowserve, Rotating Equipment Division, PO Box 25, NL-4870 AA Etten-Leur, The Netherlands. E-mail: fvisser@flowserve.com.

[1] Present address: Technical University of Eindhoven, Faculty of Mechanical Engineering, Eindhoven, The Netherlands.

0169-5983/99/$ – see front matter
PII: S0169-5983(98)00033-1

simple two-dimensional design. This flow field is discussed with respect to the flow distribution postulated by potential flow arguments and boundary-layer considerations. To that end a transparent model impeller with nine, 60°, logarithmic spiral blades was constructed, enabling non-intrusive optical flow field measurements. This test impeller, as well as the casing geometry, was designed in conformity with the theoretical work of Visser et al. (1994) to enable clarification of the essentials of fluid flow in low-specific-speed centrifugal impellers through immediate comparison with the corresponding calculations.

Studying the flow field in centrifugal impeller passages, in particular by experiment, has been the work of many turbomachinery hydrodynamicists, who – in broad outline – wished to gain insight or validate calculations in order to predict and improve (prediction of) impeller performance. The first experimental effort of note in this field was conducted by Uchimaru (1925), who reported measurements of the pressure distribution in water inside the passage of a rotating centrifugal impeller. More widely known, however, is the early experimental study of Fisher and Thoma (1932), who visualised the flow in a rotating impeller using dye injection while water was the working fluid. Other noteworthy visualisation studies on impeller passage flows are those of Fister (1966), who employed a spark-tracer method to visualise the flow of air in the passages of a radial-flow compressor, and Lennemann and Howard (1970), who utilised a hydrogen-bubble visualisation technique to investigate the flow of water in the impeller passages of a centrifugal pump running at part-capacity.

The first detailed velocity measurements were reported by Fowler (1968), who quantified the air velocity in a single, rotating, radial diffuser channel by hot-wire anemometry. Experiments quite similar to those of Fowler were also conducted by Moore (1973), whereas Howard and Kittmer (1975) used water as a working fluid and focused attention on the flow in shrouded and unshrouded impeller configurations, using a hot-film measurement technique.

Utilisation of the non-invasive laser-Doppler-velocimetry flow measurement technique (LDV) to investigate the flow inside centrifugal impellers has been reported by Miner et al. (1989), and Abramian and Howard (1994a, b). Miner et al. performed two-component LDV from the fixed non-rotating laboratory frame of reference, using a rotor-shaft encoder disk to label the absolute velocity measurements, whereas Abramian and Howard used derotator optics to measure one component of the relative fluid velocity.

For the current work, laser-Doppler velocimetry was also employed, but experimental passage flow results were obtained without employing derotator optics or rotor-shaft encoder (trigger) devices. Instead, the fluid flow in the rotating impeller passages was investigated using a custom-designed co-rotating two-component laser-Doppler velocimeter. This equipment measured directly in the rotor frame of reference, enabling simultaneous two-component LDV measurements.

The research presented in this paper compares velocity field measurements with potential-flow calculations of the flow inside the impeller passages, and focuses on the boundary-layer development along the impeller blades. Particularly, the quite substantial boundary-layer development on the suction side of the blades, which is found to be well computable by a simple direct-hierarchy approach (i.e. Truckenbrodt's integral method), will be discussed.

The measurements presented are compared to analytical calculations that are based upon the assumption of two-dimensional flow. Although this is a highly idealised physical model, it is also highly representative for impeller passage flows of radial-flow turbomachines having a low specific speed (see for instance Pfleiderer, 1991). Basically, the assumptions being (a) the fluid may be considered incompressible when dealing with pumps, fans, and hydropower turbines, (b) the importance

of the viscous forces compared to the non-viscous (inertia) forces acting on the fluid will be very small, so that the bulk of the fluid may be considered inviscid, (c) the flow enters the machine free from vorticity, and (d) the flow is restricted to depend on radial and angular coordinates only. These assumptions simplify the flow problem, leaving the essentials intact. Additionally, equiangular blades are adopted; i.e. blades having a constant angle between radius and tangent. These blades are not only mathematically convenient, but also highly representative since most radial blade designs in practice are closely represented by equiangular blades. The above-described physical model enables analytical solutions in closed form to be determined (Visser et al., 1994). The sometimes underestimated importance of such a physical model is that it forms an essential bridge between measurements and numerical models.

2. Theoretical background

In order to facilitate the understanding of the subject-matter, the two-dimensional (zeroth order) potential-flow solution for the passagewise relative fluid velocity, w_s, and its normal component, w_n, that holds asymptotically for a passage region well away from the blade tips will be briefly considered.

With reference to Fig. 1 it follows that (Visser et al., 1994)

$$w_s(r,\lambda) \sim \frac{Q}{2\pi r\cos(\beta)} + \frac{\Omega r}{\sin(\beta)}\left(\frac{\sin h(t)}{t}e^{\lambda\sin(2\beta)-t} - 1\right), \tag{1}$$

$$w_n(r,\lambda) \sim \frac{\Omega r\cos(\beta)}{\sin^2(\beta)}\left(1 - e^{\lambda\sin(2\beta)} + \frac{n\lambda}{\pi}\sin h(t)e^{\lambda\sin(2\beta)-t}\right), \tag{2}$$

as $(\cos(\beta)/s)^2 \to 0$, in which $0 \leqslant \lambda \leqslant 2\pi/n$, $t = \pi\sin(2\beta)/n$, β is the blade angle, n is the number of impeller blades, s is the solidity [2], and $Q = Q_v/b_2$ with Q_v being the volume flow rate and b_2 being the discharge height of the impeller passage.

Fig. 2 illustrates this asymptotic solution for the passage flow velocity. It shows the displacement (i.e. zero throughflow) velocity for a 60°, nine-bladed impeller. From this graph it is observed that there exists a negative passagewise velocity contribution along the pressure side ($\lambda = 2\pi/n$) of the blades due to the revolution of the impeller. This reverse-flow effect is commonly interpreted as being the result of a relative eddy located between consecutive blades; which originates from the irrotationality of the absolute flow field [3].

From Fig. 2 it further becomes evident that the normal velocity will be significantly smaller than the passagewise component, taking into account the superposition of a throughflow velocity $(Q/(2\pi r\cos(\beta)))$ such that $w_s \geqslant 0 \ \forall\lambda \in [0, 2\pi/n]$.

[2] For a radial impeller equipped with logarithmic spiral blades it follows that, $s = n(2\pi\cos(\beta))\ln(r_2/r_1)$, in which r_1 and r_2 are the impeller (blade) inner and outer tip radius, respectively; see also Brennen (1994) for a brief account on solidity.

[3] The potential-flow pattern that arises between impeller blades in the absence of throughflow, consists of rotating cells of fluid that are termed relative eddies; these eddies are the key feature with regard to rotational slip in centrifugal impellers (see also Visser et al., 1994).

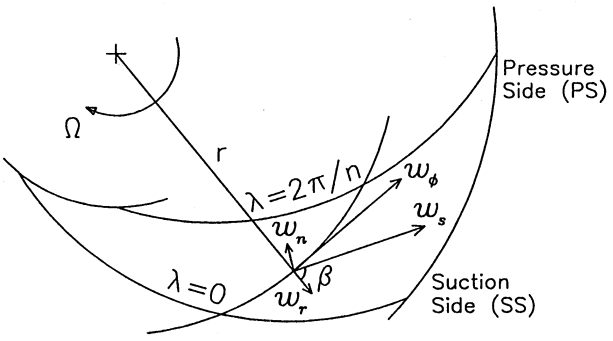

Fig. 1. Passage velocities.

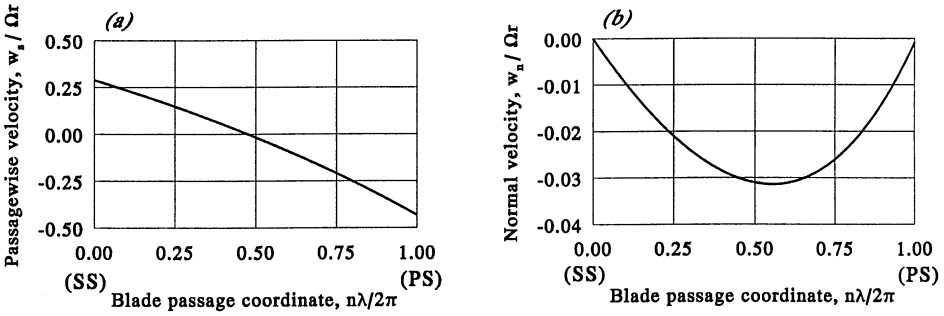

Fig. 2. Zero-throughflow impeller passage velocities according to Eqs. (1), (2) for nine, 60°, logarithmic spiral blades; (a) passagewise velocity; (b) normal velocity.

3. Experimental apparatus and technique

3.1. Test facility

The experiments were performed in the impeller-passage flow apparatus illustrated schematically in Fig. 3. This open-loop test facility was designed such that throughflow and impeller speed could be set independently, which enabled a wide range of operating points.

The test rig comprised a transparent perspex test impeller mounted horizontally between two glass windows, on a support that was fixed rigidly on a turntable that could be driven at any speed from 0 to 100 r.p.m. The volume flow rate through the impeller was controlled by means of a throttling valve in the return duct and could be set from 0 to 20 l/s. The impeller discharged in a large vaneless diffuser/volute, which was equipped with four symmetrically arranged outlets. Downstream disturbances were stemmed by a screen with 1.6% opening, placed around the test impeller at the outer perimeter of the test section. Upstream, in the impeller inlet pipe, a honeycomb type of flow straightener was installed.

A frequency-controlled circulation pump fed the settling tank with demineralised tap water from the main tank, such that the test rig operated under overflow conditions; that is, the settling tank was flooded and a small flux of water was bypassed to the main tank. The water flow rate (Q_v)

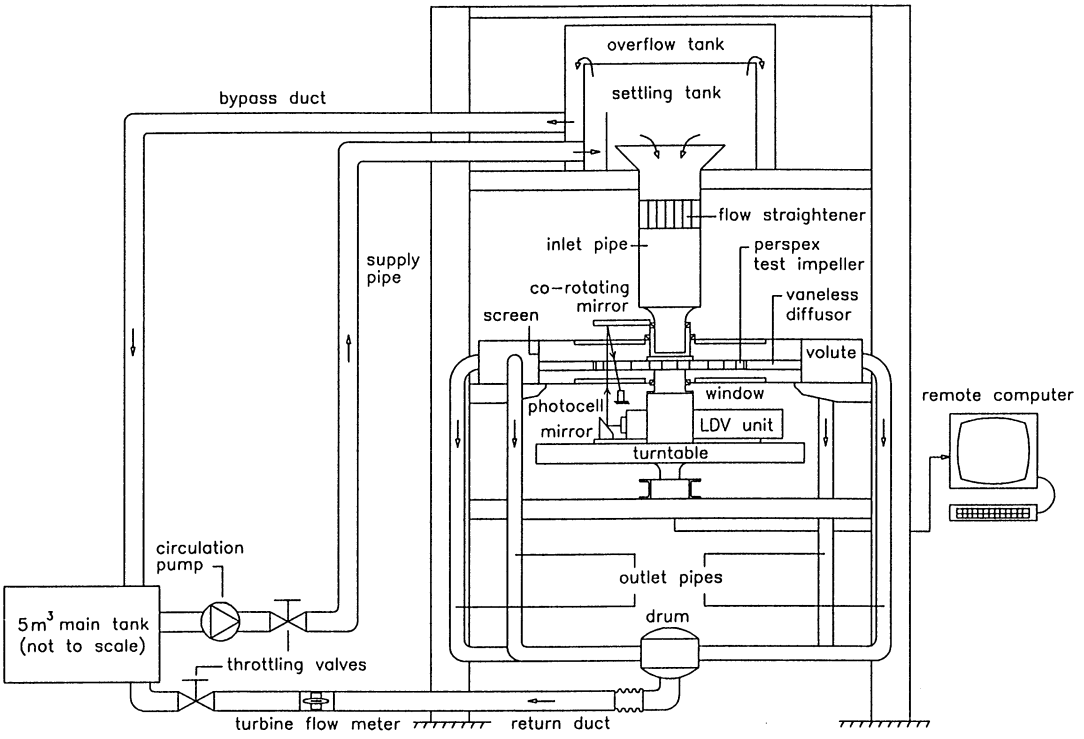

Fig. 3. Impeller-passage flow apparatus.

through the impeller was measured by a turbine flow meter in the return duct. Both the main tank and the settling tank were open to atmosphere.

3.2. The LDV system

The system that was used for the laser-Doppler-velocimetry (LDV) flow measurements was a commercial-grade two-component forward-scatter reference-beam arrangement (Fig. 4a) with combined counter-tracker signal processor, which was developed by Delft Hydraulics – The Netherlands. Key features of the arrangement were (a) high data density at good signal-to-noise ratio, (b) low laser power (6 mW), and (c) simple realisation of two-dimensional measurement system (Fig. 4b). The system was operated in its ± 1.43 m/s speed range, and functioned as follows.

In the LDV unit (Fig. 4a), a helium–neon laser provided a beam bisected by a beam splitter into a (80%) high-intensity main beam and a (20%) low-intensity secondary beam. Two Bragg cells arranged for a frequency shift of 39.4 MHz to the main beam and 40.2 MHz to the secondary beam, thus establishing an actual frequency shift of 0.8 MHz. This pre-shift eliminated directional ambiguity, so that not only the absolute value but also the direction of the velocity components could be measured. A beam displacer corrected the alignment of the secondary beam after the Bragg cell, and a second beam splitter divided the beam into two identical reference beams. These two reference beams and the main beam were focused with a 400 mm focal-depth lens, so that they intersected

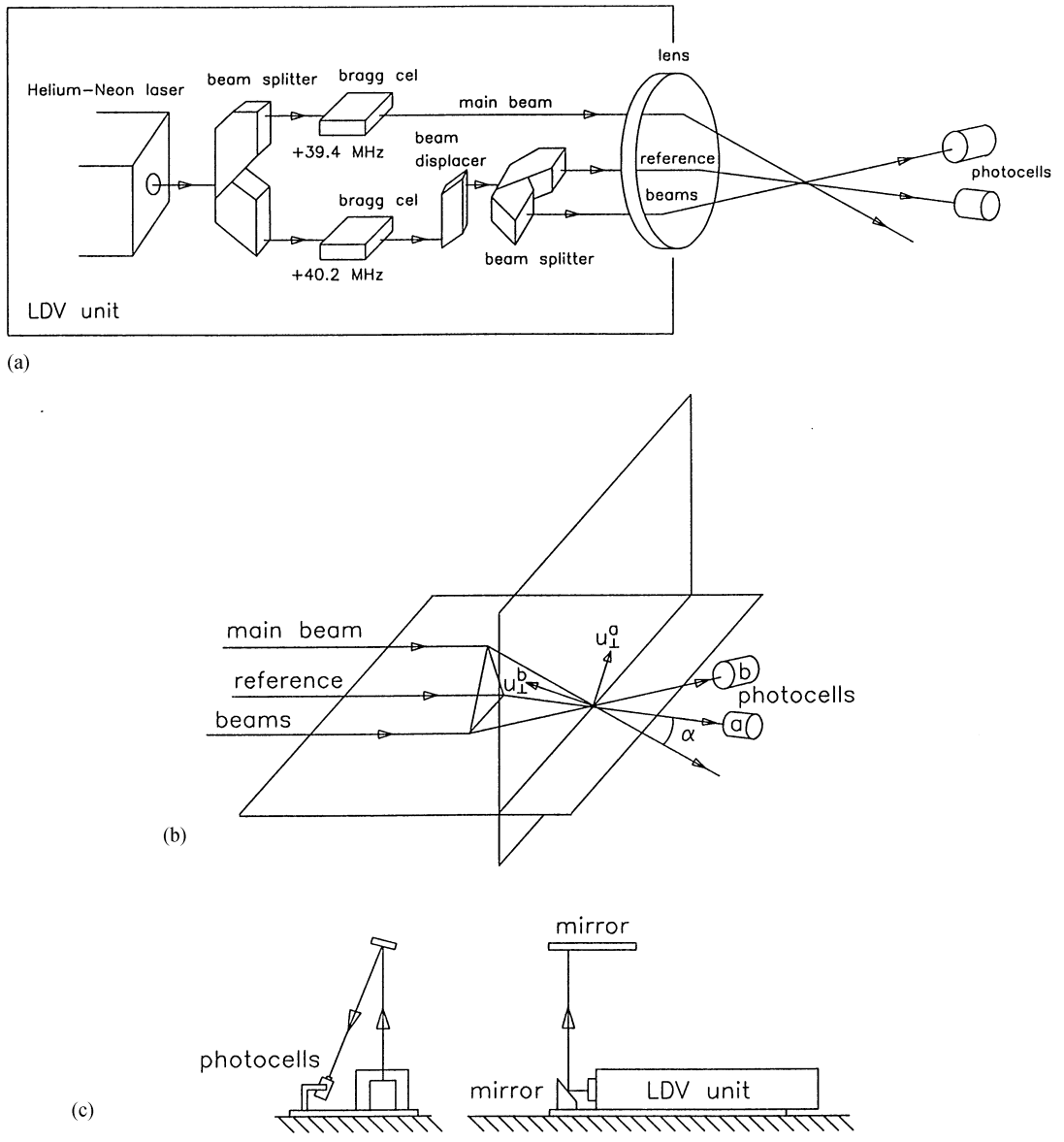

Fig. 4. The LDV system: (a) arrangement of the LDV unit and photocells; (b) principle of the two-dimensional reference-beam forward-scatter system; (c) optical bypass arrangement.

in one point, yielding two ellipsoidal measurement volumes with a beamwise length of 6.5 mm each. Two photocells detected the scatter of natural seed particles moving through the measurement volumes (Fig. 4b), while the detection signals themselves were sent to the processing unit. This signal processor contained two frequency trackers, each of them regulated by a counter; that is, the counters provided the capture range of the trackers and the matching of the signal frequency. In this way, the small capture range of the frequency trackers was overcome, while a high response rate

could still be benefited. The output signal of each tracker was a DC voltage level between −10 and 10 V.

In the experimental set-up (Fig. 3) the LDV unit was mounted on a traversing apparatus, that was stationed on the turntable and controlled remotely over a slip-ring arrangement. A mirror placed in front of the LDV unit deflected the three laser beams, so that the measurement volumes were positioned in an impeller passage (see also Fig. 4c). A second mirror, attached to the impeller front shroud reflected the post-measurement reference beams onto the photocells, which were also mounted on the traversing apparatus. The turntable further held the signal processing unit, of which the output signals were transmitted over the slip-ring arrangement to a remote computer.

With the co-rotating LDV arrangement the radial and circumferential relative (blade passage) fluid velocity could be measured simultaneously. In each of the two measurement volumes the velocity component, $u_\perp$, perpendicular to the bisector of the main beam and the respective reference beam was measured, and from these measurements the radial and circumferential components were computed by the processing unit. At the positions of measurement the two output signals of the processing unit, representing the instantaneous velocity components, were each sampled two thousand times by the remote computer at 30 Hz data rate, and from the collected samples the ensemble average and variance were computed.

4. Experimental and computational results

In the test rigs were investigated the blade passage flow of respectively, a five-, nine-, and fifteen-bladed impeller with 60°, logarithmic spiral blades. Results, however, will only be presented for the nine-bladed impeller; a complete account of the results of all three test impellers can be found in Visser (1996).

Fig. 5 shows the nine-bladed test impeller, which was designed to run at 32 r.p.m. At this angular speed, the Reynolds number based on impeller exit diameter and outlet peripheral speed equals 10^6. The (design) specific speed of the test impeller, expressed in terms of the common non-dimensional quantity $\Omega_s = \Omega Q_v^{1/2}/(gH)$, in which g is the acceleration due to gravity and H is the impeller total differential head, was of the order of 0.3; which is a typical low-specific-speed value (see for instance Brennen, 1994, or Dixon, 1978, for a discussion on specific speed).

The rotational speed of 32 r.p.m. seems rather low, but it should be recognised that the impeller has a very large outer diameter. The impeller exit peripheral speed is thus comparable to values found in practise for low speed pumps. This is expressed by the above-mentioned Reynolds number. It further should be recognised that the performance of impellers is characterised by their specific speed (Ω_s) rather than their rotational speed (Ω). In fact, a particular type of impeller (with a given Ω_s) can run theoretically at any rotational speed. This will not change its performance; that is to say, the performance will change in line with the affinity law. This law (see for instance Brennen, 1994, or Lobanoff and Ross, 1992) states that for similar conditions of flow the capacity will vary directly with the ratio of the speed, and that the head will vary with the square of this ratio. Hence, it is not necessary to test at full speed or full size. This is a very common approach for pumping machinery applications.

The results that will be presented here include measurements along several trajectories in the passages of the test impeller, at one particular operating condition near design discharge; i.e.

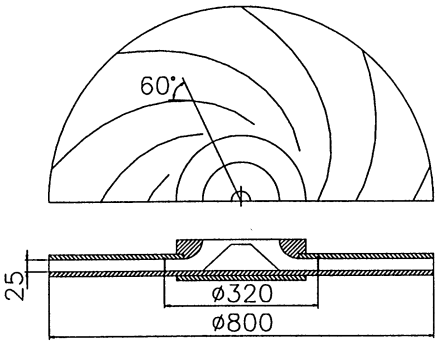

Fig. 5. Test impeller; dimensions in mm.

$\Phi = Q_v/(2\pi\Omega r_2^2 b_2) = 0.11$. The plan of discussion is first to present the LDV flow measurements of the impeller passage flows, and compare them with the corresponding potential-flow calculations. Then, attention will be focused on the viscous boundary layer on the blade suction side, where a comparison will be made between measurements and calculations employing the common thin-shear-layer approximation. The boundary-layer analysis is principally confined to the blade suction side because the LDV flow measurements particularly show that there is no significant boundary-layer (displacement) thickness on the blade pressure side.

For completeness, it is further brought to attention that a particle-image flow visualisation preceded the LDV experiments (Visser and Jonker, 1995). By observation of particle-image streak lines this study brought out clearly that the flow inside the blade passages was steady with time and unidirectional in the rotating frame, except at low off-design volume flow rates; that is, at throughflow well below the value corresponding to shockless entry. There the cyclic motion that is generally addressed as rotating stall was clearly observed (see also Fisher and Thoma, 1932, and Lennemann and Howard, 1970). This particular flow phenomenon was encountered at volume flow rates below $\Phi \approx 0.05$, at which the cycle frequency appeared to be equal to 15–20% of the rotational speed. The particle-image exploration further revealed a normal impeller passage flow with minor entrance shock near design discharge flow ($\Phi = 0.11$), whereas well above design discharge flow a leading-edge streamline discontinuity and a modest pressure-side leading-edge separation bubble were observed. In particular, it became evident from the preliminary visual tests near-design discharge that a predominant potential-flow type of fluid behaviour was actually present inside the blade passages, in that higher values of the passage velocity at the blade suction side and near stagnation flow at the blade pressure side were observed (Visser and Jonker, 1995).

4.1. Blade-to-blade impeller passage flow

Attention shall be focused here on the measured and computed fluid velocities of the blade-to-blade flow field. Results will be presented, that were obtained along radial cross-passage trajectories at passage mid-height at steady revolutionary speed and design discharge flow. Furthermore, data points obtained along circumferential cross-passage trajectories at passage mid-height will be discussed, as well as two sets of hub-to-shroud cross-sectional measurements.

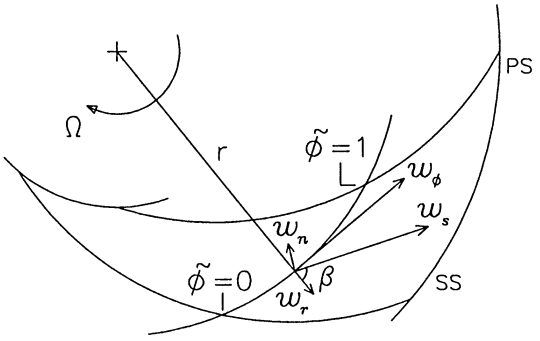

Fig. 6. System of blade-passage coordinates.

The LDV equipment measured the radial and circumferential relative velocity components w_r and w_ϕ from which the passagewise and normal components w_s and w_n were determined. The discussion, however, will be mainly confined to the passagewise velocity since only this velocity component is of present importance.

The presentation of the respective results will be done in a dimensionless form and will include both the measurement data and the corresponding calculated potential-flow results. To this end the velocities have been scaled by the impeller outlet peripheral speed (Ωr_2), while the position along the respective trajectories has been non-dimensionalised by blade-fitted co-ordinates $(\tilde{r}, \tilde{\phi}) \in [0, 1]$, defined as

$$\tilde{r} = \frac{r - r_{ps}}{r_{ss} - r_{ps}}, \tag{3}$$

$$\tilde{\phi} = \frac{\phi - \phi_{ss}}{\phi_{ps} - \phi_{ss}}, \tag{4}$$

where the respective subscripts denote suction side (ss) and pressure side (ps); see also Fig. 6. For radial trajectories in the entry and exit regions where either the pressure side or the suction side is not present, r_1 and r_2 are used instead of r_{ps} and r_{ss} to compute $\tilde{r}$.

The theoretical (potential-flow) results shown in the respective graphs have been computed principally from the solution that holds asymptotically in a region well away from the blade tips, i.e. zeroth-order expansion (1), except for those regions where the expansion does not hold; there the theoretical results were obtained from additional finite-element calculations (van Esch, 1995).

In order to compute and plot the asymptotic solution along the radial cross-passage trajectories the following relationship has been used:

$$\tilde{\phi} = 1 - \frac{n \tan(\beta)}{2\pi} \ln\left(\frac{r}{r_{ps}}\right), \tag{5}$$

which describes a radial traverse ($r_{ps} \leqslant r \leqslant r_{ss}$) in blade-fitted coordinates. The respective theoretical results are reflected by solid lines in the various figures.

The first result presented concerns the radial-traverse measurements, which are given in Fig. 7. This figure shows the (scaled) values of the passagewise velocity (w_s) along radial traverses that are

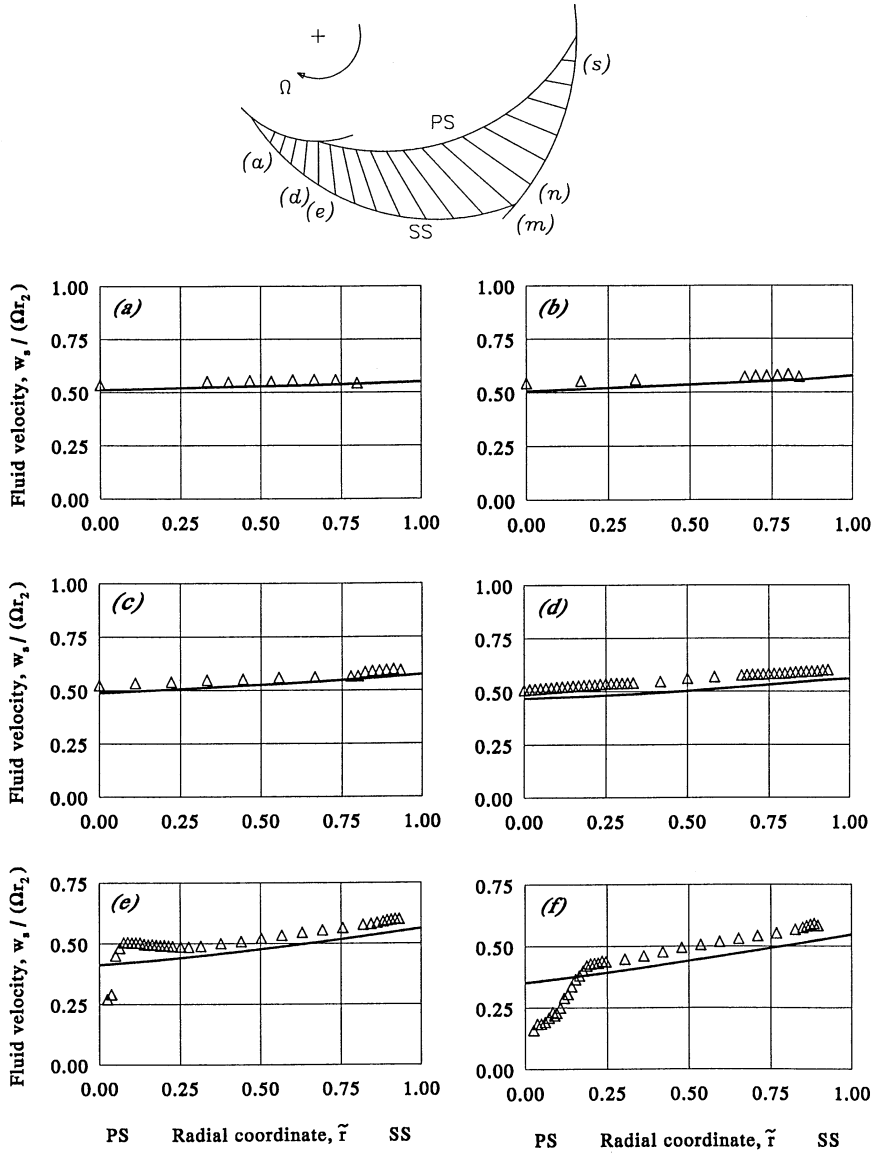

Fig. 7. Measured and computed mid-height passagewise fluid velocities at $\Phi = 0.11$; (a) $R_{ss} = 0.438$, (b) $R_{ss} = 0.475$, (c) $R_{ss} = 0.513$, (d) $R_{ss} = 0.550$, (e) $R_{ss} = 0.400$, (f) $R_{ss} = 0.434$, (g) $R_{ss} = 0.467$, (h) $R_{ss} = 0.501$, (i) $R_{ss} = 0.534$, (j) $R_{ss} = 0.568$, (k) $R_{ss} = 0.601$, (l) $R_{ss} = 0.635$, (m) $R_{ss} = 0.668$, (n) $R_{ss} = 0.700$, (o) $R_{ss} = 0.750$, (p) $R_{ss} = 0.800$, (q) $R_{ss} = 0.850$, (r) $R_{ss} = 0.900$, (s) $R_{ss} = 0.950$. Experimental data indicated by symbols; solid lines indicate computed results: (a)–(d) and (n)–(s), finite element method; (e)–(m), asymptotic expansion (1).

identified by their interception with the blade pressure side, i.e. R_{ps} $(= r_{ps}/r_2)$, or the blade suction side, i.e. R_{ss} $(= r_{ss}/r_2)$.

Next, to illustrate the low relative magnitude of the normal velocity, Fig. 8 displays the w_n to w_s ratio for the $R_{ps} = 0.568$ radial traverse. This clearly shows that in the core-flow region a relatively

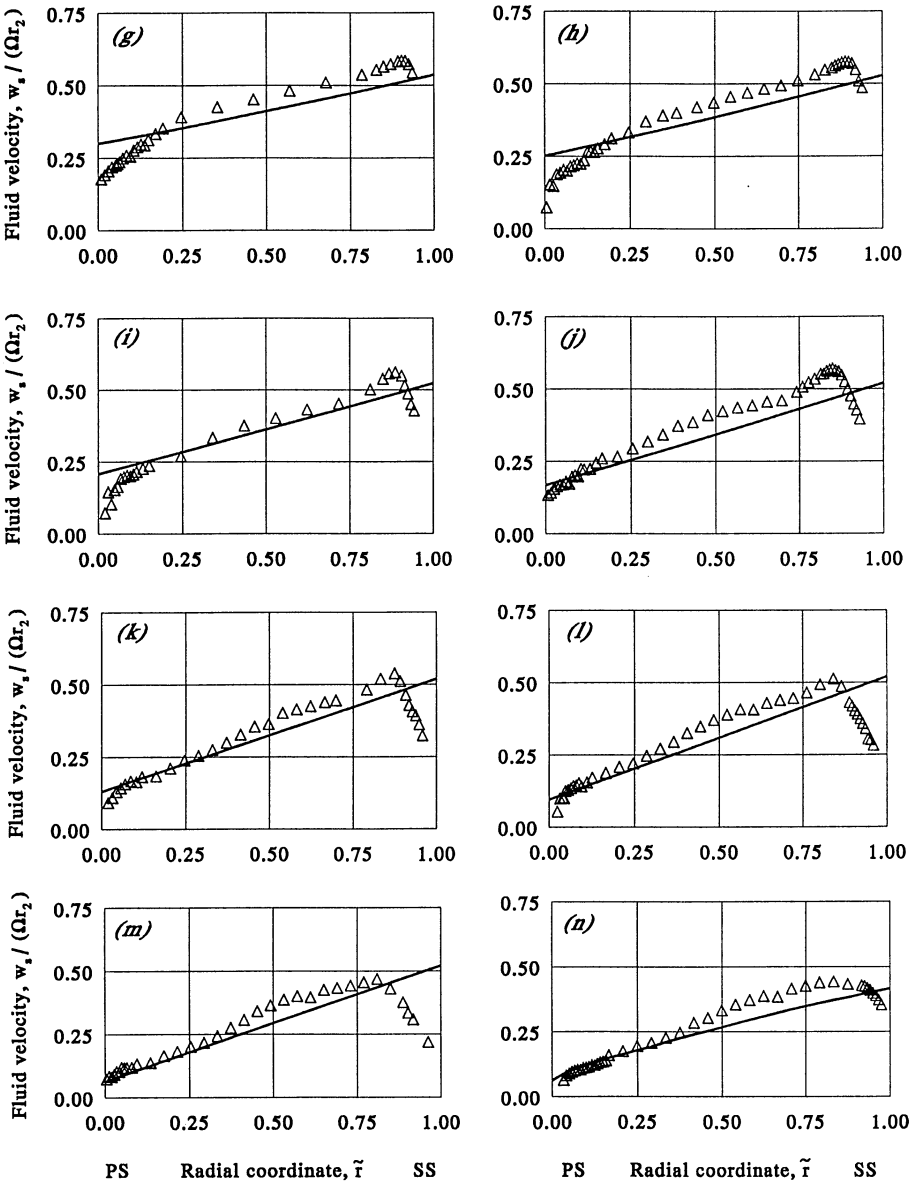

Fig. 7. Continued.

small normal velocity prevails. Only near the pressure side a comparatively high normal velocity is observed.

The last plots presented here (Figs. 9 and 10) show the circumferential cross-passage measurements. Fig. 9 shows the values of the blade-to-blade passagewise velocity at mid-height along the circumferential cross-passage trajectories, while Fig. 10 displays the cross-sectional hub-to-shroud measurements.

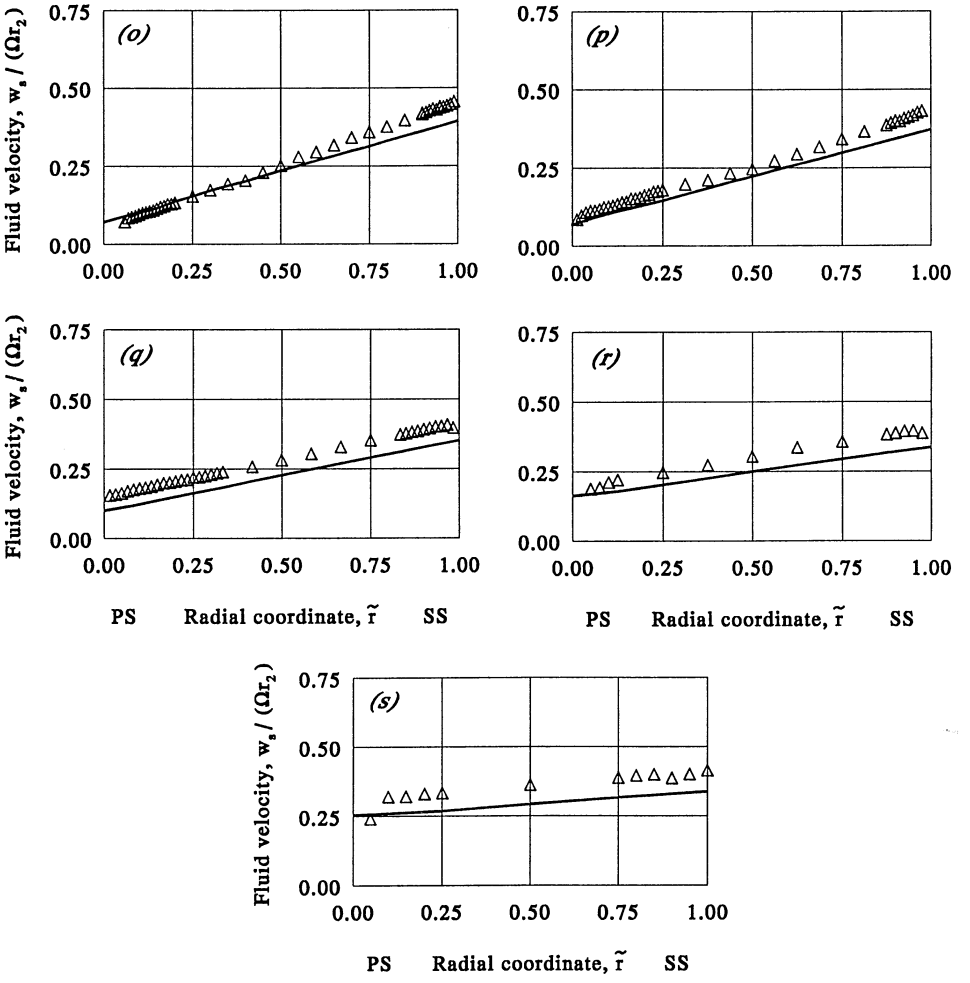

Fig. 7. Continued.

With reference to the respective plots it is seen that the measurement data compare well (for the core-flow region) with the theoretical potential-flow predictions all along the passage. This confirms that the potential-flow character is distinctly present. Near the blade surfaces it is further seen that there is a departure from the potential-flow behaviour due to the effect of viscosity. In particular, it is observed that there is a substantial development of (non-separated) viscous boundary layers along the suction side of the blades, whereas the boundary layer growth along the blade pressure side is seen to be very small. The observation that there is a very thin pressure-side boundary layer is of particular importance, since it means that the core flow will hardly be influenced, that is to say displaced, by the boundary layer on the pressure side of the blades. Stated differently, merely the development of the boundary layer along the blade suction side needs to be taken into account with regard to the displacement of the core flow. It should, however, still be recognised that the boundary layer on the blade pressure side remains to be of importance regarding the determination of the viscous drag, and by consequence, for (the prediction of) the impeller efficiency.

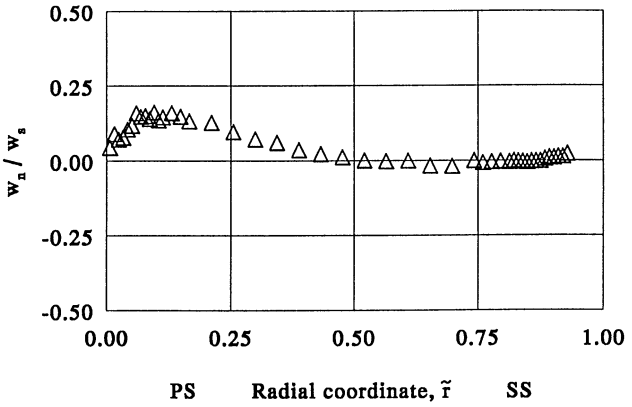

Fig. 8. Relative magnitude of the normal velocity along the traverse of $R_{ps} = 0.568$ (trajectory (j) in Fig. 7).

Lastly, completing the current discussion of the passage flow measurements, it should be noted that the cross-sectional hub-to-shroud measurements (Fig. 10) show that there is a nearly uniform velocity distribution from hub to shroud, which corroborates the assumption of two-dimensional flow for this type of impeller.

4.2. Boundary layer on blade suction side

Above, it was noted that the viscous boundary layer on the blade suction side is quite substantial in magnitude. This boundary layer will here be further discussed with respect to calculations performed in a classical way. The boundary layer on the blade pressure side was seen to be small, and will not be discussed. Furthermore, the discussion will be principally confined to the calculation of the displacement thickness.

The basic perception of the current analysis is that the common flat-wall thin-shear-layer (TSL) approximation applies also to the case of rotating low-specific-speed impellers equipped with blades of modest (sufficiently weak) curvature, so that calculations performed in the ordinary direct-hierarchy fashion can be employed to compute the blade-suction-side boundary layer. Additional conditions on the impeller speed (Ω) and the impeller-blade surface curvature to assure the validity of the assumption thereby being (see also Johnston and Eide, 1976)

$$\left|\frac{\Omega\delta}{w_e}\right| \ll 1 \quad \text{and} \quad \left|\frac{\delta}{R_c}\right| \ll 1, \tag{6}$$

in which δ denotes the boundary-layer thickness, w_e is the longitudinal edge velocity at the impeller blades, and R_c is the local radius of curvature, which for logarithmic spiral blades simply equals $r/\sin(\beta)$. Both conditions hold in most of the practical cases concerning fluid flow in centrifugal impellers. In fact, effects of system rotation and surface curvature are for those situations of fluid flow fully accommodated in the description of the core flow[4].

[4] Johnston and Eide (1976) pointed out that the TSL approximation applies as long as the mentioned parameters (6) will not get as large as 0.05.

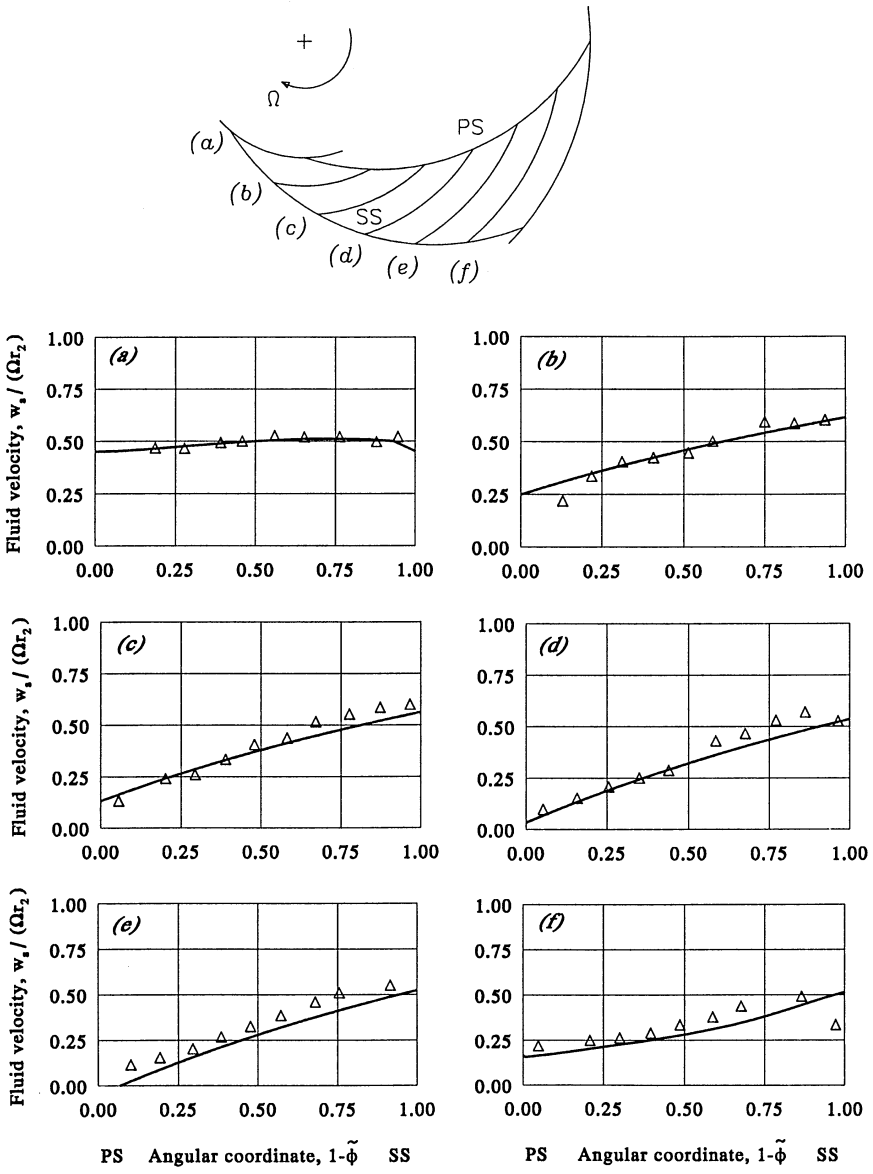

Fig. 9. Measured and computed mid-height passagewise fluid velocities at $\Phi = 0.11$ at radial distances $(r - r_1)/(r_2 - r_1)$ of (a) 0, (b) $\frac{1}{6}$, (c) $\frac{1}{3}$, (d) $\frac{1}{2}$, (e) $\frac{2}{3}$, and (f) $\frac{5}{6}$. Experimental data indicated by symbols; solid lines indicate computed results: (a) and (f), finite element method; (b)–(e), asymptotic expansion (1).

To illustrate the above-mentioned perception, the boundary-layer displacement thickness on the suction side of the blades of the test impeller has been computed at $\Omega = 32$ r.p.m. by means of the integration method due to Truckenbrodt (see for instance Schlichting, 1979, or Cebeci and Smith, 1974). By way of approximation it was thereby assumed that the turbulent boundary layer started at

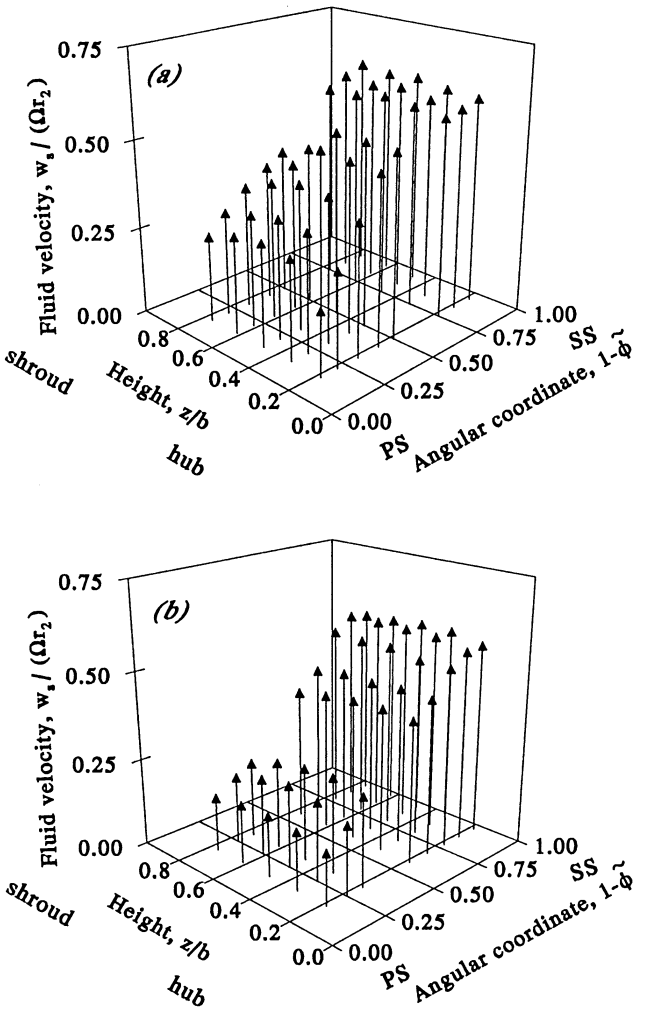

Fig. 10. Cross-sectional passagewise fluid velocities at $\Phi = 0.11$, measured at a radial distance $(r - r_1)/(r_2 - r_1)$ of (a) $\frac{1}{6}$, and (b) $\frac{1}{2}$.

$x_s = 0$, that is, without a laminar inlet portion. Furthermore, it was supposed that the shape factors equalled the value corresponding to the case of a zero pressure gradient. This is strictly speaking incorrect because of the adverse pressure gradient. However, the actual shape-factor values do not differ more than a few percent from the zero-pressure-gradient values (see also Schlichting, 1979), so that the assumption of a zero pressure gradient may be considered suitable from an engineering point of view.

The displacement thickness $\delta_1(x_s)$ thus obtained, is presented in Fig. 11. The graphs show computed values that are based on the potential-flow longitudinal edge velocity w_e, as well as calculation results derived from the measured longitudinal edge velocity (Fig. 12). Fig. 11 further shows the corresponding experimental values obtained from the LDV flow measurements, which have been

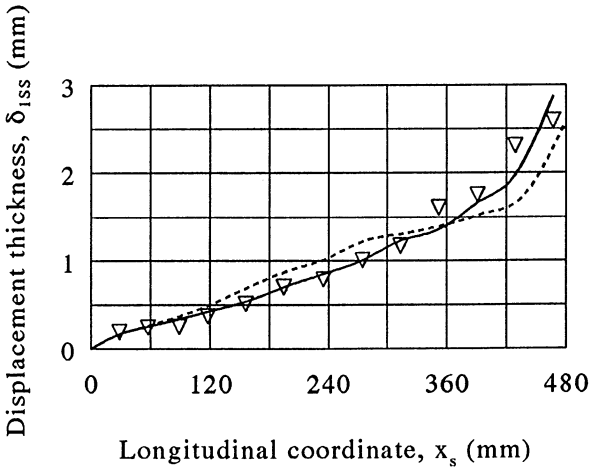

Fig. 11. Measured and calculated displacement thickness on the suction side of the blades of the test impeller at passage mid-height at design discharge. Experimental data indicated by symbols; dashed line indicates prediction from potential-flow free-stream velocity; solid line shows calculation based on measured edge velocity (see also Fig. 12).

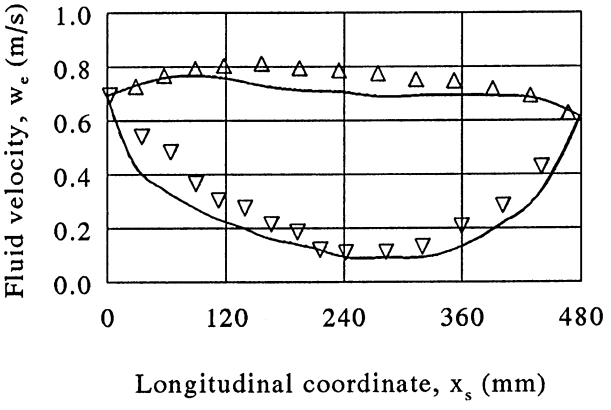

Fig. 12. Longitudinal edge velocities at the blades of the test impeller at passage mid-height at design discharge. Solid line indicates potential-flow calculation; symbols indicate experimental values: Δ, suction side; ∇, pressure side.

derived indirectly from the observed boundary-layer thickness (δ) by using the "corollary"[5] $\delta_1 \approx 0.13\delta$. From Fig. 11 it is seen that there is agreement between the experimentally obtained values of the displacement thickness and the theoretical calculations on the basis of the measured edge velocity, as for the calculations performed with the potential-flow free-stream velocities.

[5] By the law of the wake it follows that $\delta_1/\delta = (c_f/2)^{1/2}(1 + \Pi)/K$, where c_f is the skin friction coefficient, $\kappa = 0.41$, and Π is Coles' parameter, which is about 0.2 for the current case of low-Reynolds-number turbulent boundary-layers (see also Monin and Yaglom, 1971, and Cebeci and Smith, 1974). The skin-friction coefficient c_f is estimated at 0.005 ($Re_{x_s} \approx 2 \times 10^5$) by applying the formula of Schultz-Grunow, i.e. $c_f = 0.370(\log(Re_{x_s}))^{-2.584}$; see for instance Schlichting (1979), p. 643, or Monin and Yaglom (1971), p. 324.

In conclusion, taking into consideration the findings of this section, it can be said that there is little reason to doubt whether the well-established ordinary approaches may be applied to calculate the boundary-layer on the suction side of the blades of a low-specific-speed centrifugal impeller, like the one in this paper. Only at high operating speeds, and for cases of strong blade-surface curvature, so that the conditions $|(\Omega\delta)/w_e| \ll 1$ and $|\delta/R_c| \ll 1$ are severely violated, it seems natural to expect that application of common direct-hierarchy flat-plate (TSL) approximations will yield improper results. Furthermore, it is emphasised that the passage flows are not fully developed turbulent channel flows, but merely potential-flow core flows with thin low-Reynolds-number turbulent boundary layers on the blade-passage walls; provided, of course, that the passages are sufficiently wide with regard to the displacement due to the boundary-layer growth. In the event that the latter is not the case, the potential-flow concept still remains applicable, but one has to take into account the relative magnitude of the displacement thickness; that is, re-compute the potential-flow free-stream velocity by incorporating the initial estimate of the displacement.

5. Concluding remarks

Based on laser-Doppler-velocimetry flow measurements in the rotor frame of reference, the flow inside the passages of a radial nine-bladed low-specific-speed model centrifugal impeller with 60°, logarithmic spiral blades has been investigated.

From the experimental results it has been shown that the core of the blade passage flow is well described by two-dimensional potential-flow theory at design discharge. Particularly, the presence of the potential-flow relative eddy, which is responsible for the rotational slip in centrifugal impellers, has been corroborated in line with potential-flow theory by higher values of the passage velocities in the proximity of the blade suction side and near-stagnation flow at the blade pressure side.

Next, the measurements have exposed that only the boundary layer on the blade suction side is substantial in magnitude, contrary to the one on the blade pressure side. This is particularly important to note, as one may neglect under normal operating conditions, to a first approximation, the pressure-side displacement thickness.

Lastly, it has been demonstrated that the boundary layer (i.e. the displacement thickness) on the blade suction side can be computed by application of ordinary direct-hierarchy flat-plate boundary-layer theory, indicating that effects of system rotation and blade-surface curvature are well accommodated in the potential-flow description for the type of impeller considered here.

Acknowledgement

The authors gratefully acknowledge the financial support by SHELL, The Netherlands, enabling execution of the experimental programme.

References

Abramian, M., Howard, J.H.G., 1994a. A rotating laser-Doppler anemometry system for unsteady relative flow measurements in model centrifugal impellers. ASME J. Turbomachinery 116, 260–268.

Abramian, M., Howard, J.H.G., 1994b. Experimental investigation of the steady and unsteady relative flow in a model centrifugal impeller passage. ASME J. Turbomachinery 116, 269–279.

Brennen, C.E., 1994. Hydrodynamics of Pumps, Oxford University Press, Oxford.

Cebeci, T., Smith, A.M.O., 1974. Analysis of Turbulent Boundary Layers, Academic Press, New York.

Dixon, S.L., 1978. Fluid Mechanics, Thermodynamics of Turbomachinery, Pergamon Press, Oxford.

Esch van, B.P.M., 1995. Private communication; see also Esch, van B.P.M., Kruyt, N.P., Jonker, J.B., 1995. An efficient method for computing three-dimensional potential flows in hydraulic turbomachines. In: Proc. 9th Int. Conf. on Finite Elements in Fluids. Venice, Italy, pp. 633–644.

Fisher, K., Thoma, D., 1932. Investigation of the flow conditions in a centrifugal pump. Trans. ASME HYD-54-8, 141–155.

Fister, W., 1966. Sichtbarmachung der Strömungen in Radialverdichterstufen, besonders der Relativströmung in rotierenden Laufrädern, durch Funkenblitze. Brennstoff-Wärme-Kraft 18, 425–429.

Fowler, H.S., 1968. The distribution and stability of flow in a rotating channel. ASME J. Eng. Power 90, 229–236.

Howard, J.H.G., Kittmer, C.W., 1975. Measured passage velocities in a radial impeller with shrouded and unshrouded configurations. ASME J. Eng. Power 97, 207–213.

Johnston, J.P., Eide, S.A., 1976. Turbulent boundary layers on centrifugal compressor blades: prediction of the effects of surface curvature and rotation. ASME J. Fluids Eng. 98, 374–381.

Lennemann, E., Howard, J.H.G., 1970. Unsteady flow phenomena in rotating centrifugal impeller passages. ASME J. Eng. Power 92, 65–72.

Lobanoff, V.S. Ross, R.R., 1992. Centrifugal Pumps: Design & Application, Gulf Publishing Company, Houston.

Miner, S.M., Beaudoin, R.J., Flack, R.D., 1989. Laser velocimeter measurements in a centrifugal flow pump. ASME J. Turbomachinery 111, 205–212.

Monin, A.S., Yaglom, A.M., 1971. Statistical Fluid Mechanics: Mechanics of Turbulence, MIT Press, Cambridge, MA.

Moore, J., 1973. A wake and eddy in a rotating, radial-flow passage. Part 1: experimental results. ASME J. Eng. Power 95, 205–212.

Pfleiderer, C., 1991. Strömungsmachinen, Springer, Berlin.

Schlichting, H., 1979. Boundary-Layer Theory, McGraw-Hill, New York.

Uchimaru, S., 1925. Experimental Research on the Distribution of Water Pressure in a Centrifugal Impeller. In: Tokyo Imperial University, J. Fac. Eng. 16, 157–169.

Visser, F.C., Brouwers, J.J.H., Badie, R., 1994. Theoretical analysis of inertially irrotational and solenoidal flow in two-dimensional radial-flow pump and turbine impellers with equiangular blades. J. Fluid Mech. 269, 107–141.

Visser, F.C., Jonker, J.B., 1995. Investigation of the relative flow in low specific speed model centrifugal pump impellers using sweep-beam particle image velocimetry. In: Proc. 7th Int. Symp. on Flow Visualization. Seattle, Washington, pp. 654–659.

Visser, F.C., 1996. On the flow in centrifugal impellers, Thesis, University of Twente.